Drug mechanism enrichment analysis interprets rank-ordered drug lists to facilitate biological understanding

Belinda B. Garana[1], James H. Joly[1,†], Alireza Delfarah[1,‡], Hyunjun Hong[2], and Nicholas A. Graham[1,3,4]

[1]Mork Family Department of Chemical Engineering and Materials Science, University of Southern California, Los Angeles, CA, USA

[2]Department of Computer Science, Information Systems, and Applications, Los Angeles City College, Los Angeles, CA, USA

[3]Norris Comprehensive Cancer Center, University of Southern California, Los Angeles, CA, USA

[4]Leonard Davis School of Gerontology, University of Southern California, Los Angeles, CA, USA

[†]Current address: Nautilus Biotechnology, San Carlos, CA, USA

[‡]Current address: Calico Life Sciences, South San Francisco, CA

Running title:

Drug Mechanism Enrichment Analysis

Keywords: Drug discovery; Drug repurposing; Precision medicine; Mechanism of action; Targeted therapeutics; Enrichment analysis; Gene expression analysis; Proteomic analysis; Senescence; Senolytic.

To whom correspondence should be addressed:

Nicholas A. Graham, University of Southern California, 3710 McClintock Ave., RTH 509, Los Angeles, CA 90089. Phone: 213-240-0449; E-mail: nagraham@usc.edu

ABSTRACT

There is a pressing need for improved methods to identify effective therapeutics for disease. Many computational approaches have been developed to predict drugs based on molecular signatures. However, extracting biological or mechanistic insight from these tools remains a challenge because they often produce long, rank-ordered lists of candidate drugs that are difficult to interpret. Here, we developed Drug Mechanism Enrichment Analysis (DMEA), an approach to generate biological insight from rank-ordered drug lists by identifying enriched sets of drugs that share a common mechanism of action. The method is based on Gene Set Enrichment Analysis (GSEA) and derives its power by integrating prior knowledge about the mechanisms of action (MOAs) and/or molecular targets of individual drugs. To test our approach, we first demonstrated that DMEA can successfully identify an enriched drug MOA in simulated data. Next, we validated DMEA using three types of rank-ordered drug lists including gene expression connectivity scores, cell viability connectivity scores, and weighted gene voting molecular classification scores of intrinsic and acquired drug resistance. For all these test cases, DMEA successfully detected the enrichment of the expected MOA and other MOAs of interest. Finally, to demonstrate how DMEA can generate hypotheses regarding other biological processes, we predicted senescence-inducing and senolytic drug MOAs for primary human mammary epithelial cells. We then experimentally validated the DMEA-generated hypothesis that EGFR inhibitors are senolytic in primary human mammary epithelial cells. Taken together, our results show that DMEA is a highly versatile bioinformatic tool which can identify enriched drug MOAs in rank-ordered drug lists to facilitate biological understanding. DMEA is publicly available as both a web application and an R package at https://belindabgarana.github.io/DMEA.

INTRODUCTION

Despite technological advances, identifying effective therapeutics for disease remains a pressing challenge. Recent efforts in large-scale ‘omic profiling [1–4], pharmacological and genetic loss-of-function screening [5–7], and drug perturbation profiling [8] have generated a wealth of molecular data characterizing large numbers of cell lines and their responses to perturbations. Many computational approaches have been developed to leverage these molecular data to predict drug sensitivity or similarity [9–23], and these efforts have successfully identified drugs for a wide variety of diseases, including HIV [18], osteoporosis [24], diabetes [25], and cancer [14,26,27].

Notwithstanding their great promise for precision medicine, one shortcoming of many drug prediction algorithms is that they output a long, rank-ordered list of drugs from which it is difficult to extract biological or mechanistic insight. Often, many individual drugs pass the threshold for statistical significance, and it is difficult to identify global trends, such as the coordinated enrichment of multiple drugs with a common molecular target. In addition, analysis of single drugs is subject to misinterpretation due to any known or unknown off-target toxicities.

Because large-scale pharmacological screens often include multiple inhibitors with the same molecular target (e.g., EGFR, HMGCR, proteasome, etc.), we reasoned that a method which incorporates known mechanisms of action (MOAs) could facilitate biological interpretation of the rank-ordered drug lists generated by common drug prediction algorithms. This concept is analogous to how Gene Set Enrichment Analysis (GSEA) enhances biological interpretation of transcriptomic data by leveraging knowledge of which genes belong to biological pathways, processes, or diseases [28]. Simply put, if most of the drugs that share an MOA are found at the top of the rank-ordered drug list, then we can have increased confidence that the enriched MOA represents a true, on-target drug sensitivity or similarity. Our tool Drug Mechanism Enrichment

Analysis (DMEA) quantifies this enrichment and outputs relevant data and plots to enable users to qualitatively verify and understand the results. By facilitating the biological interpretation of rank-ordered drug lists via a user-friendly web application and R package, DMEA will help researchers identify therapeutic mechanisms of action for disease.

METHODS

Drug Mechanism Enrichment Analysis (DMEA)

DMEA tests whether drugs that share a common MOA are enriched in a rank-ordered drug list. DMEA can be used on any rank-ordered list of drugs with MOA annotations representing at least two MOAs. In order for a drug MOA to be evaluated by DMEA, at least six drugs must be annotated with that MOA (or the minimum number of drugs per MOA set by the user). Each drug must be ranked by a nonzero numeric value. The method uses a GSEA-like algorithm [28] to identify drug MOAs which are overrepresented at either end of the input rank-ordered drug list. If a drug MOA is positively enriched, then drugs annotated with that MOA are overrepresented at the top of the list. Conversely, if a drug MOA is negatively enriched, then drugs which share that MOA annotation are overrepresented at the bottom of the list.

For each MOA, DMEA calculates an enrichment score (ES) as the maximum deviation from zero of a running-sum, weighted Kolmogorov-Smirnov-like statistic. The p-value is estimated using an empirical permutation test wherein drugs are randomly assigned MOA labels in 1,000 independent permutations to calculate a distribution of null enrichment scores (ES_null); the p-value is then calculated as the percentage of same-signed ES_null equal to or greater than the ES divided by the percentage of same-signed ES_null. The normalized enrichment score (NES) is then calculated by dividing the ES by the mean of the same-signed portion of the ES_null distribution. Finally, the q-value or false discovery rate (FDR) is calculated as the percentage of

same-signed NES in the null distribution (i.e., NES_null) with NES equal or greater to the observed NES divided by the percentage of same-signed NES equal or greater. Per the recommendation for GSEA, we use a significance threshold of $p < 0.05$ and FDR < 0.25. Given a rank-ordered drug list, DMEA generates 1) enrichment results for all tested drug MOAs; 2) a volcano plot summarizing the NES and $-\log_{10}$(p-value) for all tested drug MOAs; and 3) mountain plot(s) for individual drug MOA(s) which pass the user-provided FDR cutoff (Fig. 1).

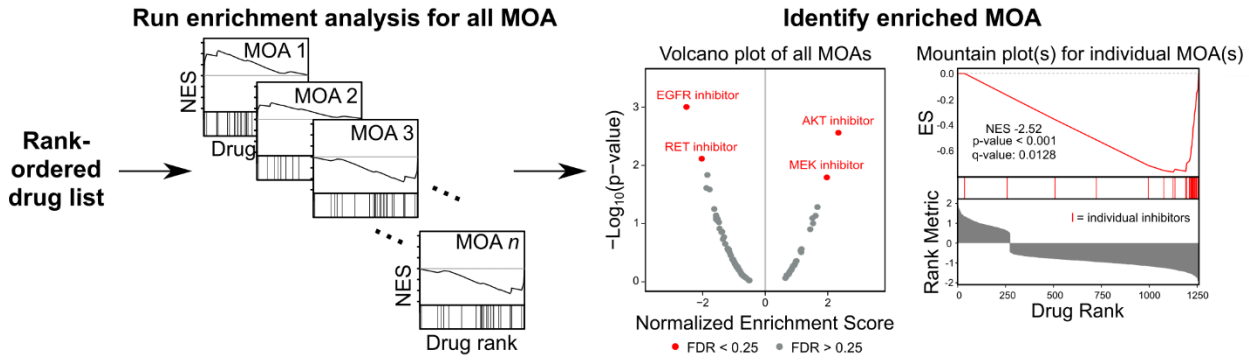

Figure 1. Overview of Drug Mechanism Enrichment Analysis. DMEA is a versatile GSEA-like algorithm which analyzes a rank-ordered drug list to identify drug MOAs which are overrepresented at either end of the input drug list. Given a rank-ordered drug list where drugs have been annotated with known MOAs, DMEA runs an enrichment analysis for each individual MOA. After calculating p-values and FDR q-values, DMEA outputs 1) a data frame of enrichment results for all tested drug MOAs; 2) a volcano plot summarizing the NES and $-\log_{10}$(p-value) for all tested drug MOAs; and 3) mountain plot(s) for individual drug MOA(s) which pass the FDR cutoff.

Simulation study of DMEA

To evaluate the sensitivity of DMEA, we first simulated a rank-ordered drug list by randomly assigning values from a normal distribution ($\mu = 0$, $\sigma = 0.5$) for 1,351 drugs with MOA annotations in the PRISM drug screen. Next, a number of drugs, X, were randomly sampled as a synthetic drug set and their rank values were selected from a shifted normal distribution ($\mu = Y$, $\sigma = 0.5$); the size of the synthetic drug set, X, was varied from 5 to 50 drugs, and the perturbation value Y was varied from -1 to +1. This rank-ordered drug list was then analyzed by DMEA to

determine the enrichment of the synthetic drug set relative to the known drug MOA sets provided by the PRISM drug screen. For each pair of *X* and *Y* values, the simulation was repeated 50 times to assess reproducibility.

CMap L1000 Query

The Connectivity Map (CMap) web portal (https://clue.io) [8] allows users to query the L1000 gene expression database using 10 to 150 input up- and down-regulated gene IDs. The output is a normalized connectivity score which indicates the similarity between the query and differentially expressed gene sets induced by drug treatments. A positive score indicates similarity between the query and the perturbagen signature, whereas a negative score indicates dissimilarity. Specifically, we used the "query.gct" file from the zip file output by the CMap L1000 Query, including the MOA annotations provided in the file. Since this file includes results for various cell lines in the L1000 database as well as information for quality control, we removed any scores indicated to be low quality and averaged scores for each drug having MOA annotations. Here, we used example data sets from the CMap web portal, including: 1) GSE32547, HUVEC cells treated with the HMGCR inhibitor pitavastatin (1 μM, 4h) or DMSO [29]; 2) GSE35230, A375 melanoma clones treated with the MEK inhibitor GSK212 (30 nM, 24 h) or DMSO [30]; 3) GSE14003, JEKO1 cells treated with the proteasome inhibitor bortezomib (10 h) or untreated [31]; 4) GSE28896, human CD34+ cells treated with the glucocorticoid agonist dexamethasone (24 h) or untreated [32]; and 5) GSE33643, A2058 cells treated with the PI3K/MTOR inhibitor BEZ235 (3 doses at 24 h) or DMSO [33]. We also used the up- and down-regulated biomarkers from a proteomic signature of senescence in primary human mammary epithelial cells (HMECs) [34].

CMap PRISM Query

The Connectivity Map (CMap) web portal (https://clue.io) [8], also allows users to query PRISM viability data [5] for 3 to 489 input cell line IDs classified as having "UP" or "DOWN" phenotypes. The query outputs a normalized connectivity score ranking the drugs based on their toxicity towards the "UP" versus "DOWN" cell lines. A positive score indicates toxicity towards "UP" cell lines, whereas a negative score indicates toxicity towards "DOWN" cell lines or lack of toxicity towards "UP" cell lines. In particular, we used the "ncs.gct" file from the zip file output by the CMap PRISM Query, including the MOA annotations provided in the file. Again, we only considered drugs with MOA annotations. Here, we used examples provided by the CMap web portal including: 1) cell lines with the EGFR activating mutation p.E746_A750del (i.e., "UP" cell lines: NCIH1650, PC14, and HCC827); 2) cell lines with high expression of *PDGFRA* (i.e., "UP" cell lines: 42MGBA, A204, A2780, G292CLONEA141B1, G402, GB1, HS618T, KNS42, LMSU, MG63, MON, NCIH1703, SBC5, SKNAS, SNU685, SW579, U118MG, U251MG, and YH13); and 3) cell lines sensitive to the HMGCR inhibitor lovastatin (i.e., "UP" cell lines: HUH28, SNU1079, MG63, LOXIMVI, MDAMB231, SF295, SNU1105, YKG1, ACHN, HCT15, SNU423, SNU886, CALU1, HCC4006, HCC44, HCC827, NCIH1915, NCIH661, NCIH838, PC14, RERFLCMS, SQ1, SW1573, KYSE150, A2780, COV434, JHOM1, MCAS, KP3, SW1990, MSTO211H, YD15, HS944T, MDAMB435S, MELJUSO, A204, HT1080, RH30, LMSU, FTC238, YD8, 5637, and AGS).

Weighted gene voting (WGV)

To calculate a molecular classification score for cell lines based on external molecular signatures, we used weighted gene voting (WGV) [35]. The WGV score is the dot product between an external gene signature of interest and normalized RNAseq expression values for 327 adherent cancer cell lines from the Cancer Cell Line Encyclopedia (CCLE, version 19Q4) [3]. In

this study, we analyzed four independent transcriptomic signatures, three derived from datasets for intrinsic resistance to EGFR inhibitors and one derived from a dataset for acquired resistance to a RAF inhibitor. For each transcriptomic data set, we used the R package limma [36] to perform an eBayes statistical analysis for differential expression comparing sensitive and resistant samples. Then, the top 500 genes based on $|\log_2(\text{fold-change})|$ with q-value < 0.05 were used for WGV (with the $\log_2(\text{fold-change})$ being the gene "weight" or rank value).

For gene signatures of EGFR inhibitor sensitivity, we used data sets GSE12790 [37], GSE31625 [38], and Coldren et al. [39]. For GSE12790, cell lines were classified as sensitive to erlotinib (EC50 < 1 μM: HDQ-P1, CAL85-1, and HCC1806) or resistant to erlotinib (EC50 > 10 μM: CAL-51, CAL-120, MDA-MB-231, BT-20, HCC1569, EFM-192A, HCC1954, MDA-MB-453, BT474, HCC1428, T47D, ZR-75-1, KPL-1, BT-483, MDA-MB-415, HCC1500, CAMA-1, and MCF7). For GSE31625, we used 17 transcriptomic profiles from 3 cell lines sensitive to erlotinib (H1650, H3255, and PC-9) and 12 profiles of 2 cell lines resistant to erlotinib (A549 and UKY-29). Finally, based on classifications from Coldren *et al.*, we used CCLE RNAseq profiles of 5 cell lines sensitive to gefitinib (NCIH1650, HCC95, NCIH1975, NCIH1648, and NCIH2126) and 7 cell lines resistant to gefitinib (NCIH520, NCIH460, NCIH1299, HCC44, A549, NCIH1703, and HCC15). For a gene signature of RAF inhibitor sensitivity, we used dataset GSE66539 with paired biopsy samples of melanoma from 3 patients before vemurafenib treatment and after emergence of resistance to vemurafenib [40].

DMEA using WGV molecular classification scores

For rapid identification of drug MOAs with toxicity towards cells represented by an input gene signature, DMEA can be used in combination with a molecular classification method such as WGV, correlations, and large public databases for gene expression and drug screens. To do this, we accessed the Cancer Cell Line Encyclopedia version 19Q4 for RNAseq data and

calculated WGV scores for 327 adherent cancer cell lines using external molecular signatures. To avoid overfitting, we did not include WGV scores from any cell lines that had been used to generate the external molecular signature. Next, we calculated the Pearson correlation between the WGV scores and PRISM drug sensitivity scores (i.e., area under the curve (AUC) values for cell viability as a function of drug concentration) for each drug [5] using data from the most recent PRISM screen available (e.g., HTS002, MTS005, MTS006, and MTS010). Lastly, drugs were ranked by the Pearson correlation coefficient, and the rank-ordered drug list was analyzed by DMEA.

Simulation study of DMEA using WGV molecular classification scores

For 200 synthetic cell lines, we sampled drug sensitivity scores for 1,351 drugs from a bimodal mixture of two normal distributions (μ_1=0.83, σ_1=0.08 and μ_2=1.31, σ_2=0.08) with the lower distribution containing 72% of all drugs. This distribution was chosen to reflect the distribution of the PRISM drug sensitivity data (i.e., AUC) [5]. Additionally, we simulated gene expression for each cell line by sampling from a normal distribution with a mean (μ) of 0 and standard deviation (σ) of 0.5. This distribution was chosen to reflect the distribution of the normalized CCLE RNAseq data [3].

To introduce a synthetic association between gene expression and drug sensitivity, we randomly sampled a synthetic gene set of 25 genes and a synthetic drug set of 10 drugs. Next, expression values for the synthetic gene set and sensitivity scores for the synthetic drug set were each sampled from a shifted distribution, where the magnitude of the shift for each synthetic cell line is determined by a perturbation value ranging from 0 (no perturbation) to 0.1. For example, for a perturbation value of 0.1, the mean gene expression for the 25 perturbed genes in cell line 1 was μ = -0.1, and the mean sequentially increased by 0.001 for cell lines 2-200; similarly, the mean drug sensitivity of cell line 1 to the 10 perturbed drugs was shifted by -0.1, and this shift

value sequentially increased by 0.001 for cell lines 2-200. This created a gradient of perturbations in the 200 cell lines, meaning cell line 1 had the largest negative perturbation and cell line 200 had the largest positive perturbation. Then, we calculated WGV scores for each cell line by taking the dot product of the expression values of the synthetic gene set and the difference in average gene expression between the top and bottom 10 percent of cell lines (i.e., gene weights from cell lines 181-200 which had the highest mean expression versus cell lines 1-20 which had the lowest mean expression). Afterwards, we calculated the Pearson correlation between the WGV and drug sensitivity scores for each of the 1,351 drugs in the synthetic dataset. Finally, drugs were ranked by their Pearson correlation coefficient, and DMEA was performed to measure the enrichment of the synthetic drug set. To assess reproducibility, this entire process was repeated 50 times.

Cell culture

HMEC cells were purchased from Thermo Scientific and cultured in M87A medium (50% MM4 medium and 50% MCDB170 supplemented with 5 ng/ml EGF, 300 ng/ml hydrocortisone, 7.5 µg/ml insulin, 35 µg/ml BPE, 2.5 µg/ml transferrin, 5 µM isoproterenol, 50 µM ethanolamine, 50 µM o-phosphoethanolamine, 0.25 % FBS, 5 nM triiodothyronine, 0.5 nM estradiol, 0.5 ng/ml cholera toxin, 0.1 nM oxytocin, 1% anti-anti, no AlbuMax) in atmospheric oxygen. Glucose and glutamine-free DMEM was purchased from Corning (90-113-PB), Ham's F12 was purchased from US Biological (N8542-12), and MCD170 medium was purchased from Caisson Labs (MBL04). Glucose and glutamine were added to the media at the appropriate concentration for each media type. At each passage, cells were lifted with TrypLE at 80-90% confluency and seeded at a density of $2.3 \times 10^3/cm^2$.

Cell viability experiments

Proliferating HMECs (PD ~12) were seeded at a concentration of $2.1 \times 10^3/cm^2$ or $9.5 \times 10^3/cm^2$ for DMSO and triapine treatment, respectively. The following day, cells were treated with

DMSO (vehicle control) or 2 µM triapine for 3 days. The cells were counted and then treated with either DMSO (vehicle control), dacomitinib, AZD8931, or navitoclax at 100 nM or 500 nM for 3 days. Cell viability and live cell number were measured with trypan blue assay using a TC20 automated cell counter (Bio-Rad). Chemical inhibitors were from Sigma (triapine) or MedChemExpress (dacomitinib, AZD8931, navitoclax).

RESULTS

DMEA identifies an enriched drug MOA in simulated data

To evaluate the sensitivity of DMEA, we tested it on a normally distributed, synthetic drug rank list (see Methods). For a randomly sampled set of drugs ranging in size from 5 to 50 drugs, we shifted these drugs' rankings by a perturbation value ranging from -1 to 1. Next, we ran DMEA using the full rank list of 1,351 drugs to assess enrichment of the synthetic drug set. This process was repeated 50 times for each synthetic drug set size, after which the average normalized enrichment score and the percentage of replicates with significant enrichment of the synthetic drug set were visualized as heatmaps (Fig. 2).

As expected, we observed no significant enrichment of the synthetic drug set when no perturbation was added (i.e., false discovery) except for very small drug sets (i.e., 5 drugs, 2% of replicates with FDR < 0.25). As the magnitude of the perturbation was increased or decreased, the average NES of the synthetic drug set increased or decreased, respectively. Likewise, the percentage of replicates passing the significance threshold of FDR < 0.25 increased as the magnitude of the perturbation increased. These results demonstrate that DMEA can successfully identify an enriched set of drugs in simulated data.

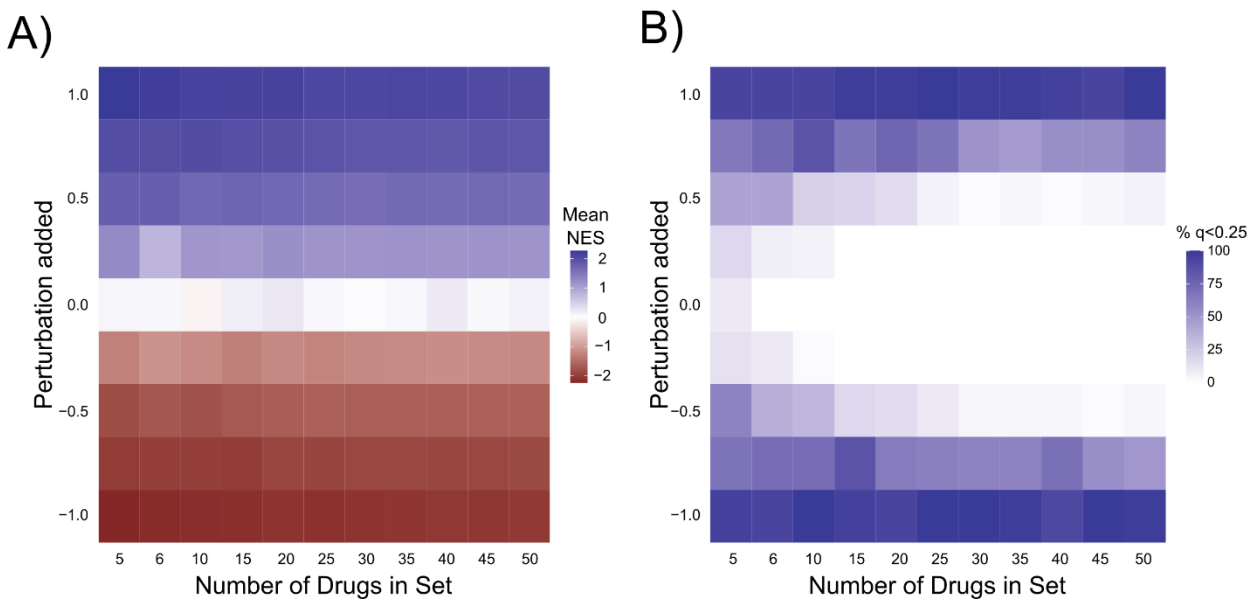

Figure 2. Sensitivity analysis of DMEA using synthetic data. Synthetic rank-ordered drug lists were generated with varying perturbations (y-axis) of different drug set sizes (x-axis), then analyzed by DMEA (see Methods). For each combination of drug set size and perturbation value, 50 replicates were performed. A) Heatmap showing the average DMEA NES for the perturbed drug set. B) Heatmap showing the percent of DMEA replicates with FDR q-value < 0.25 for the perturbed drug set.

DMEA identifies similar MOAs based on gene expression connectivity scores

Next, we sought to test whether DMEA could identify enriched drug MOAs in rank-ordered drug lists generated by the Connectivity Map (CMap), [8] a popular tool for drug discovery that contains >1 million gene expression signatures measured using a reduced representation transcriptomic profiling method termed L1000. To test DMEA, we analyzed example data sets from the CMap L1000 Query tool to identify perturbagen signatures that are similar or dissimilar to an input gene set. First, we used a gene expression signature from HUVEC cells treated with pitavastatin, an inhibitor of 3-hydroxy-3-methylglutaryl-CoA reductase (HMGCR) [29]. As expected, DMEA identified the HMGCR MOA as the only significantly positively enriched MOA in the rank-ordered list of connectivity scores (Fig. 3A). Next, we tested a gene expression signature from A375 melanoma clones treated with the MEK inhibitor GSK212 [30]. Again, DMEA correctly identified that MEK inhibitors were the most significantly positively enriched MOA in the rank-

ordered list of drug connectivity scores (Fig. 3B). Then, we analyzed a gene expression signature from JEKO1 mantle cell lymphoma cells treated with the proteasome inhibitor bortezomib [31], and DMEA accurately found that proteasome inhibitors were the most significantly positively enriched MOA (Fig. 3C). Finally, we used DMEA to test data sets from human CD34+ cells treated with the glucocorticoid agonist dexamethasone [32] and A2058 melanoma cells treated with the PI3K/MTOR inhibitor BEZ235 [33]. In both cases, DMEA correctly identified the expected positive MOA enrichment (glucocorticoid receptor agonist and PI3K/mTOR inhibitor MOAs, respectively) in rank-ordered drug lists (Supp. Fig. 1). These results show that DMEA can correctly identify enriched MOAs in rank-ordered lists of gene expression connectivity scores generated by the CMap.

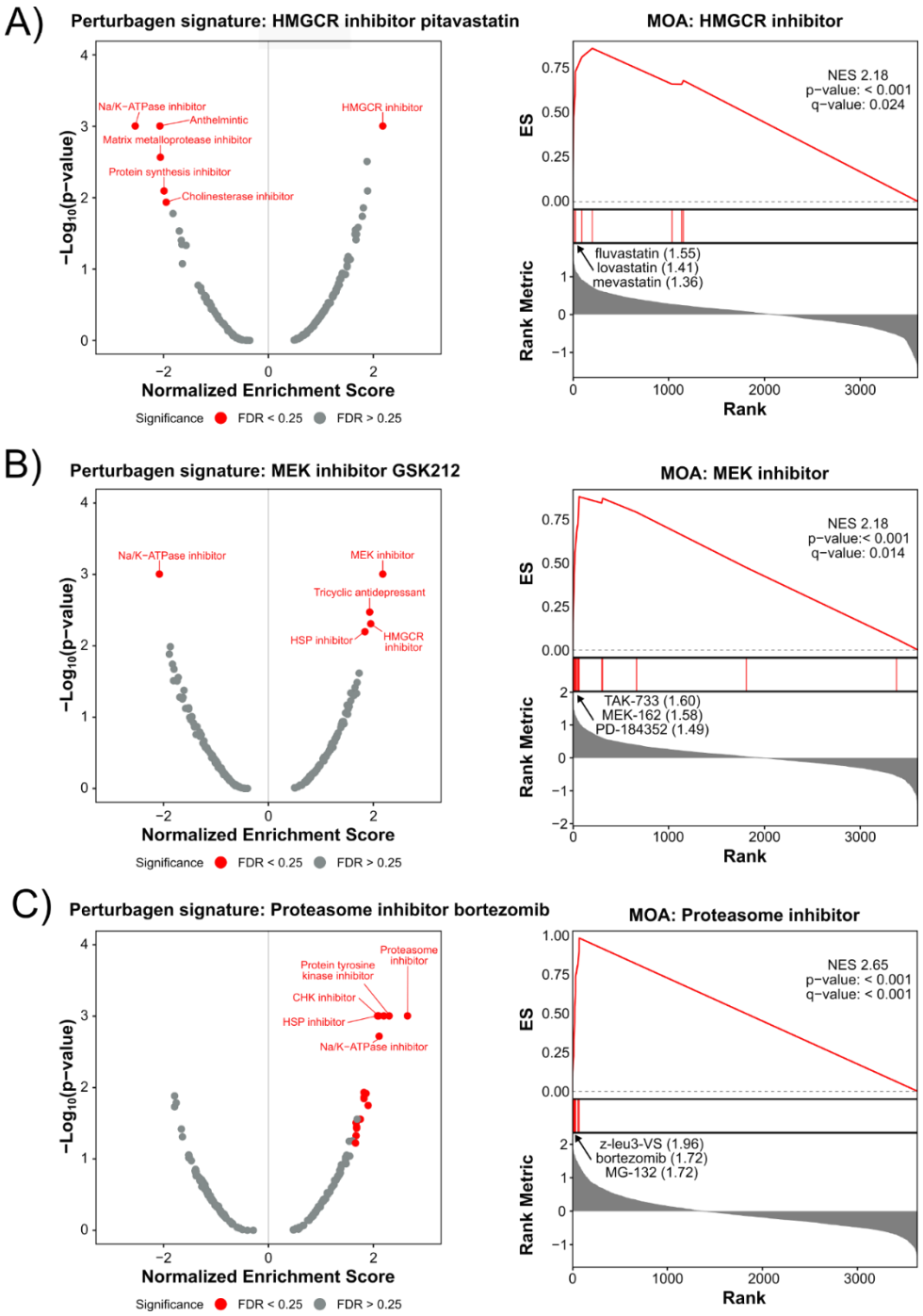

Figure 3. DMEA identifies similar MOAs based on gene expression connectivity scores. Rank-ordered drug lists were generated by querying the CMap L1000 gene expression perturbation signatures and then analyzed by DMEA. A) HUVEC cells treated with the HMGCR inhibitor pitavastatin [29], B) A375 melanoma clones treated with the MEK inhibitor GSK212 [30], and C) JEKO1 cells treated with the proteasome inhibitor bortezomib [31]. Volcano plots summarizing the NES and -$\log_{10}$(p-value) for all tested drug MOAs and mountain plots of the expected MOAs are shown. Red text indicates MOAs with p-value < 0.05 and FDR < 0.25. For each mountain plot, the inhibitors with the most positive connectivity scores are highlighted.

DMEA identifies selectively toxic MOAs based on cell viability connectivity scores

To evaluate if DMEA can identify selectively toxic drug MOAs, we used the CMap PRISM Query tool to query data from the PRISM drug repurposing database [5]. Given an input list of cell lines, the CMap PRISM Query generates a list of ~1,200 drugs ranked by normalized connectivity scores which represent the predicted sensitivity of the input cell lines to each drug. The higher the normalized connectivity score, the more toxic the drug is predicted to be for the input cell lines. Again, we analyzed example data sets from the CMap PRISM Query tool to test DMEA, including: 1) cell lines with the activating EGFR mutation p.E746_A750del, 2) cell lines with high expression of *PDGFRA*, and 3) cell lines with sensitivity to the HMGCR inhibitor lovastatin. As hypothesized, DMEA identified EGFR inhibitors (Fig. 4A), PDGFR inhibitors (Fig. 4B), and HMGCR inhibitors (Fig. 4C), respectively, as significantly positively enriched in these rank-ordered drug lists. Taken together, these examples demonstrate that DMEA can identify enriched MOA in rank-ordered lists of cell viability connectivity scores generated by CMap Query of the PRISM drug screen.

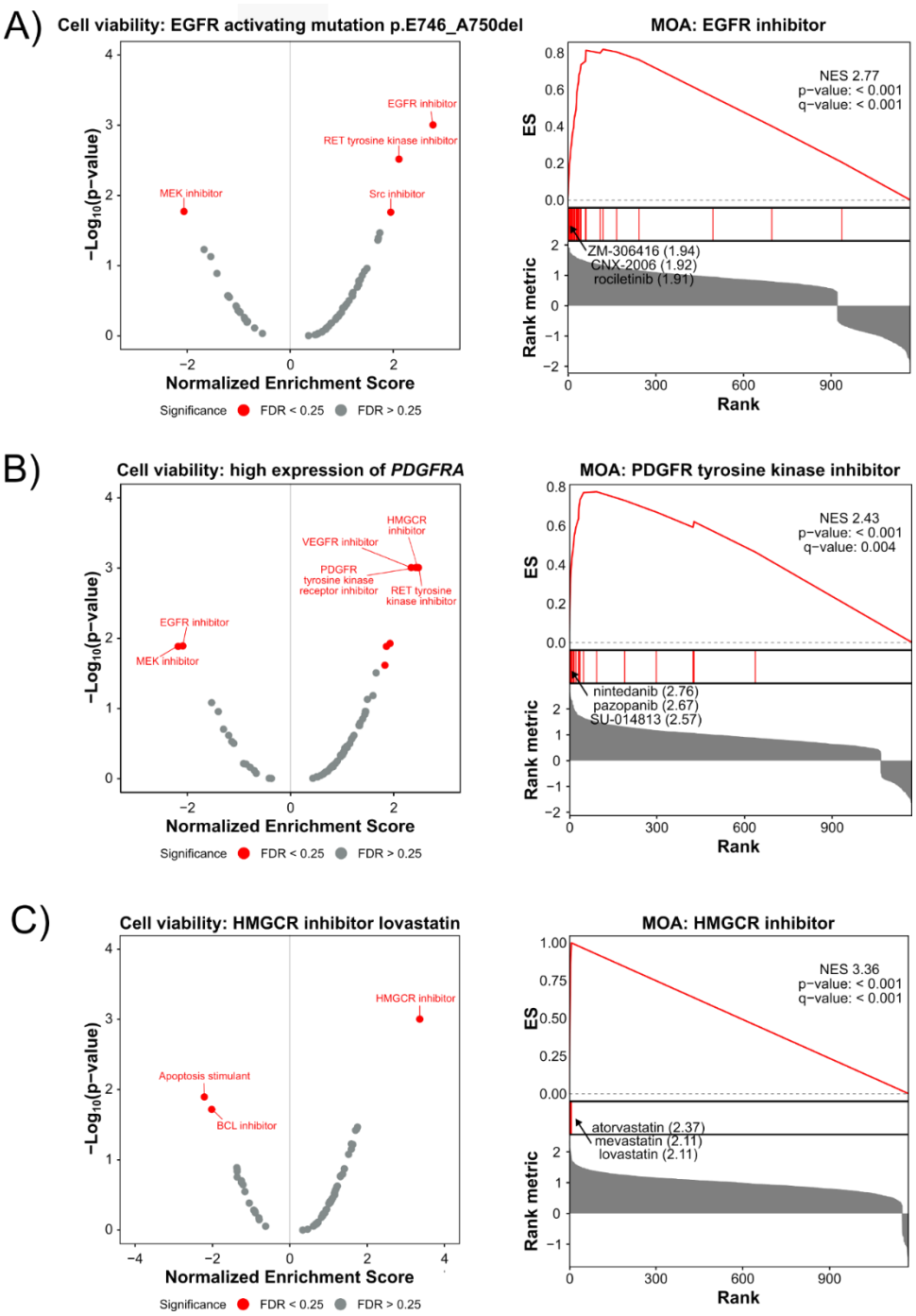

Figure 4. DMEA identifies selectively toxic MOAs based on cell viability connectivity scores. Rank-ordered drug lists were generated by querying the PRISM database with input cell line sets characterized by A) the activating EGFR mutation p.E746_A750del, B) high expression of *PDGFRA*, and C) sensitivity to the HMGCR inhibitor lovastatin. Volcano plots summarizing the NES and -$\log_{10}$(p-value) for all tested drug MOAs and mountain plots of the expected MOAs are shown. Red text indicates MOAs with p-value < 0.05 and FDR < 0.25. For each mountain plot, the inhibitors with the most positive connectivity scores are highlighted.

DMEA identifies selectively toxic MOAs based on molecular signatures

For targeted therapeutics, it would be highly desirable to use DMEA to identify selectively toxic drug MOAs given an input molecular signature (i.e., up- or down-regulated genes that characterize a disease or cell type). Though the CMap L1000 Query ranks drugs based on an input gene list, it does not consider drug toxicity. Similarly, although the CMap PRISM Query considers drug toxicity, it accepts an input of cell lines rather than genes. Therefore, to translate an input molecular signature (i.e., genes ranked by numeric weight values) into a rank-ordered list of drug sensitivity for analysis by DMEA, we leveraged a simple molecular classification method to generate a computationally fast approach that would be accessible through our user-friendly web application and R package. Specifically, we: 1) used weighted gene voting (WGV) to classify adherent cancer cell lines in the CCLE database based on similarity to an input gene signature; 2) correlated WGV scores with drug sensitivity scores (i.e., AUC) for each of 1,351 drugs in the PRISM database; and 3) ranked drugs by the correlation coefficient of WGV scores and drug AUC values (Supp. Fig. 2, see Methods).

To test this approach, we first performed a simulation study. Specifically, we simulated gene expression and drug sensitivity scores for 200 cell lines by randomly sampling values from distributions that reflected the CCLE RNAseq and PRISM drug sensitivity data. Next, to create a synthetic association between gene expression and drug sensitivity, we perturbed a subset of the gene expression data and drug sensitivity scores. We then ran 50 replicates to determine if DMEA could consistently identify enrichment of the synthetic drug set in this simulated data. To visualize the results, we plotted the average normalized enrichment score (NES) and the percent of replicates which pass the significance threshold of FDR < 0.25 as heatmaps (Supp. Fig. 3). Importantly, when there was no perturbation in drug sensitivity (AUC), the tested drug set was never significantly enriched (0% of replicates) regardless of the size of the perturbation in RNA expression. This demonstrates that DMEA is not prone to false positive results using this WGV-

based approach. In addition, increasing the perturbation in either RNA expression or drug sensitivity led to increased enrichment scores (i.e., average NES) and increased significance (i.e., higher percentage of significant replicates). These results illustrate that DMEA can successfully identify associations between gene expression and drug sensitivity with high reproducibility in simulated data.

Next, we tested whether DMEA could successfully identify drug MOAs with selective toxicity using published transcriptomic signatures of drug resistance. First, we tested three different signatures of intrinsic resistance to EGFR inhibitors: 1) non-small cell lung cancer (NSCLC) cell lines treated with erlotinib (GSE31625) [38]; 2) breast cancer cell lines treated with erlotinib (GSE12790) [37]; and 3) NSCLC cell lines treated with gefitinib (Coldren *et al.*) [39]. Notably, there was little overlap in the genes used for WGV (GSE12790 and Coldren *et al.* share zero genes, GSE12790 and GSE31625 share 11 genes, and GSE31625 and Coldren *et al.* share 14 genes). Despite differences in the gene signatures, all three analyses correctly identified EGFR inhibitors as toxic towards the cancer cell lines known to be sensitive to EGFR inhibition (Fig. 4A-B, Supp. Fig. 4). In addition, DMEA revealed consistent results across all three signatures for drug MOAs predicted to be toxic for cancer cell lines resistant to EGFR inhibitors, including HMGCR and MDM inhibitors (Fig. 4C, Supp. Fig. 4C and F). These results support that DMEA can identify selectively toxic drug MOAs given a molecular signature of intrinsic drug resistance.

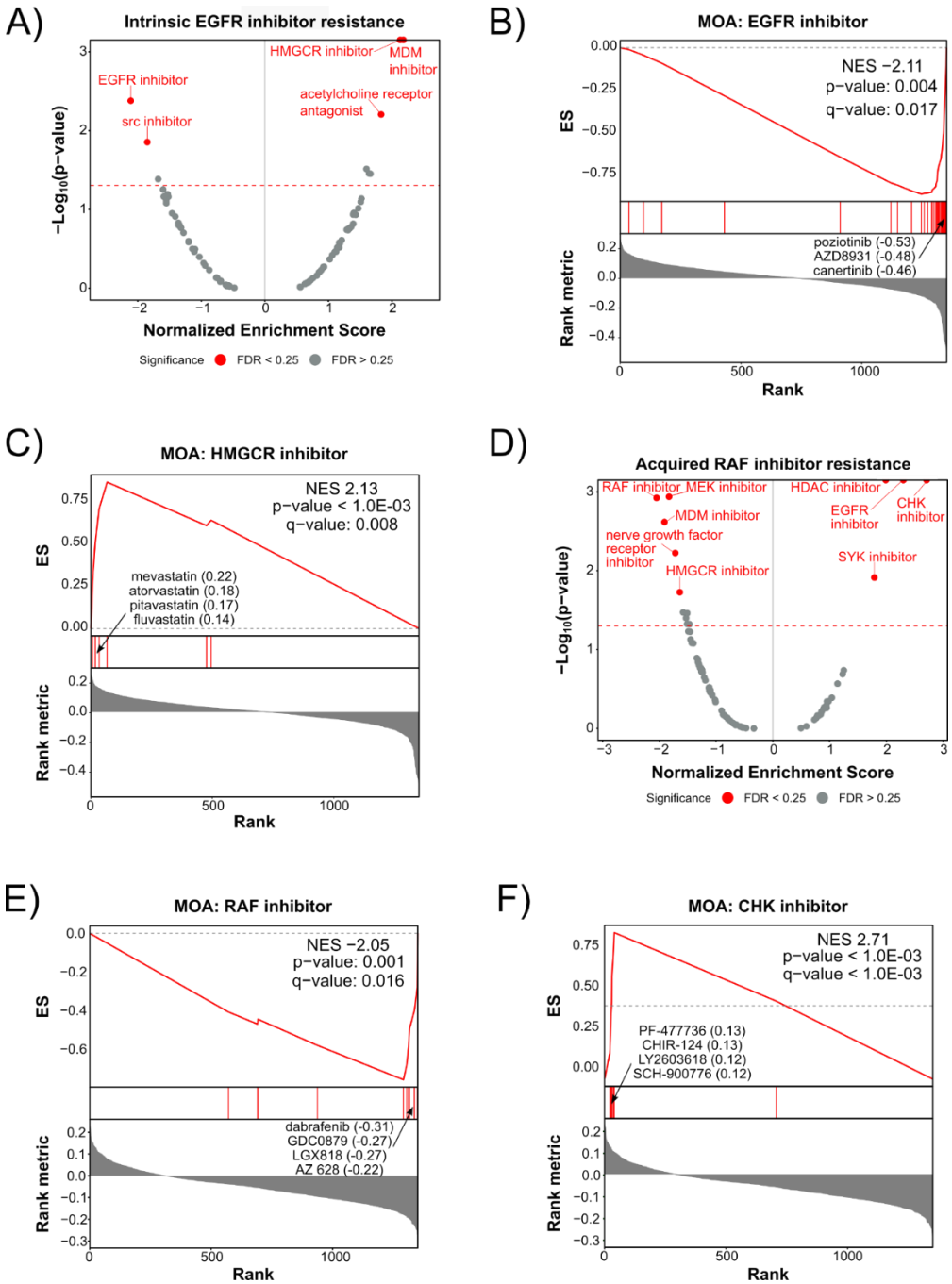

Figure 5. DMEA identifies selective toxic MOAs based on external gene expression signatures of intrinsic EGFR inhibitor resistance and acquired RAF inhibitor resistance, respectively. Using gene expression signatures of intrinsic erlotinib resistance (GSE12790 [37]) and acquired vemurafenib resistance (GSE66539 [40]), we calculated WGV molecular classification scores for 327 adherent cancer cell lines in the CCLE database. For each signature, the WGV scores were correlated with drug sensitivity scores (i.e., AUC) for 1,351 drugs from the PRISM database. Drugs were then ranked by Pearson correlation coefficient, and DMEA was performed to identify selectively toxic MOAs. A) Volcano plot of NES versus -$\log_{10}$(p-value) for DMEA using the GSE12790 signature of intrinsic erlotinib resistance. Red text indicates MOAs with p-value < 0.05 and FDR < 0.25. B) Mountain plot showing that DMEA identified the EGFR

inhibitor MOA as negatively enriched in the rank-ordered drug list generated using the GSE12790 signature of intrinsic erlotinib resistance. The most negatively correlated EGFR inhibitors are highlighted along with their correlation coefficients. C) Mountain plot showing that DMEA identified the HMGCR inhibitor MOA as positively enriched in the rank-ordered drug list generated using the GSE12790 signature of intrinsic erlotinib resistance. The most positively correlated HMGCR inhibitors are highlighted along with their correlation coefficients. D) Volcano plot of NES versus -$\log_{10}$(p-value) for DMEA using the GSE66539 signature of acquired vemurafenib resistance. Red text indicates MOAs with p-value < 0.05 and FDR < 0.25. E) Mountain plot showing that DMEA identified the RAF inhibitor MOA as negatively enriched in the rank-ordered drug list generated using the GSE66539 signature of acquired vemurafenib resistance. The most negatively correlated RAF inhibitors are highlighted along with their correlation coefficients. F) Mountain plot showing that DMEA identified the CHK inhibitor MOA as positively enriched in the rank-ordered drug list generated using the GSE66539 signature of acquired vemurafenib resistance. The most positively correlated CHK inhibitors are highlighted along with their correlation coefficients.

Furthermore, we tested whether DMEA could identify selectively toxic drug MOAs given a transcriptomic signature of acquired drug resistance. Specifically, we analyzed RNAseq data from patient biopsies of BRAF-mutant melanoma before treatment with the BRAF inhibitor vemurafenib and after the development of acquired resistance [40]. Again, DMEA correctly identified the RAF inhibitor MOA as toxic to the samples collected before resistance was acquired (Fig. 4D-E). Additionally, inhibitors of HDAC, EGFR, CHK, and SYK were identified as possibly beneficial for tumors with acquired resistance to RAF inhibition. Conversely, DMEA identified that drugs inhibiting MEK, MDM, nerve growth factor receptor, and HMGCR may be toxic towards tumors which are sensitive to RAF inhibitors (Fig. 4D). These results demonstrate that DMEA can identify acquired resistance in tumors and even predict drug MOAs which might benefit resistant tumors.

DMEA predicts senescence-inducing and senolytic drug MOAs for primary human mammary epithelial cells

Lastly, we sought to demonstrate how DMEA can be used as a discovery tool. As an example, we analyzed our recently published proteomic signature of replicative senescence, a stress-induced irreversible growth arrest associated with aging, in primary human mammary epithelial cells (HMECs) [34]. First, we performed a CMap L1000 Query using the gene names

for the up- and down-regulated proteins to predict drug MOAs that could induce senescence in HMECs. Using the CMap results, DMEA revealed positive enrichment for MOAs including proteasome, HDAC, HMGCR, and MDM inhibitors (Fig. 6A), suggesting that treatment with drugs from these MOAs may induce senescence in primary HMECs. Among the MOAs with significant negative enrichments were Na/K-ATPase inhibitors and matrix metalloprotease inhibitors, suggesting that these drug MOAs might antagonize senescence in primary HMECs.

Secondly, we analyzed the same proteomic signature of senescence with our own WGV-based method to identify selectively toxic MOAs based on the input molecular signature (Supp. Fig. 2). In contrast to analysis of the CMap L1000 Query which identified MOAs which induce similar gene expression, this DMEA pipeline instead predicted drug MOAs that may be toxic to cells with similar gene expression as senescent HMEC (i.e., senolytic MOAs). Using this approach, we found that the EGFR and MEK inhibitor MOAs were significantly positively enriched in the rank-ordered drug list (Fig. 6B). This suggests that compounds from these MOAs may be senolytic in HMECs. Among the negatively enriched drug MOAs which may be more toxic to non-senescent, proliferating HMECs, we found MDM inhibitors, bromodomain inhibitors, and other MOAs.

To experimentally test the hypothesis that EGFR inhibitors exhibit selective toxicity against senescent HMECs, we used a drug-induced model of senescence where the RRM2 inhibitor triapine induces HMECs to senesce [41]. We treated proliferating and senescent HMECs with DMSO (negative control), the EGFR inhibitor dacomitinib, the EGFR inhibitor AZD8931, or the known senolytic compound navitoclax (positive control) at 100 and 500 nM. After 3 days of treatment, dacomitinib, AZD8931, and navitoclax significantly reduced the viability of senescent but not proliferating HMECs at both concentrations (Fig. 6C). Additionally, all three drugs reduced the total number of viable senescent cells. Notably, low concentrations of dacomitinib and

navitoclax (100 nM) were selectively toxic to senescent cells without affecting the growth rate of non-senescent, proliferating HMECs. In contrast, although 100 nM of AZD8931 was selectively toxic to senescent HMEC, AZD8931 also reduced the growth rate of proliferating, non-senescent HMECs. These experimental results support that the EGFR inhibitors dacomitinib and AZD8931 are novel senolytic compounds in HMECs, validating a hypothesis generated by DMEA.

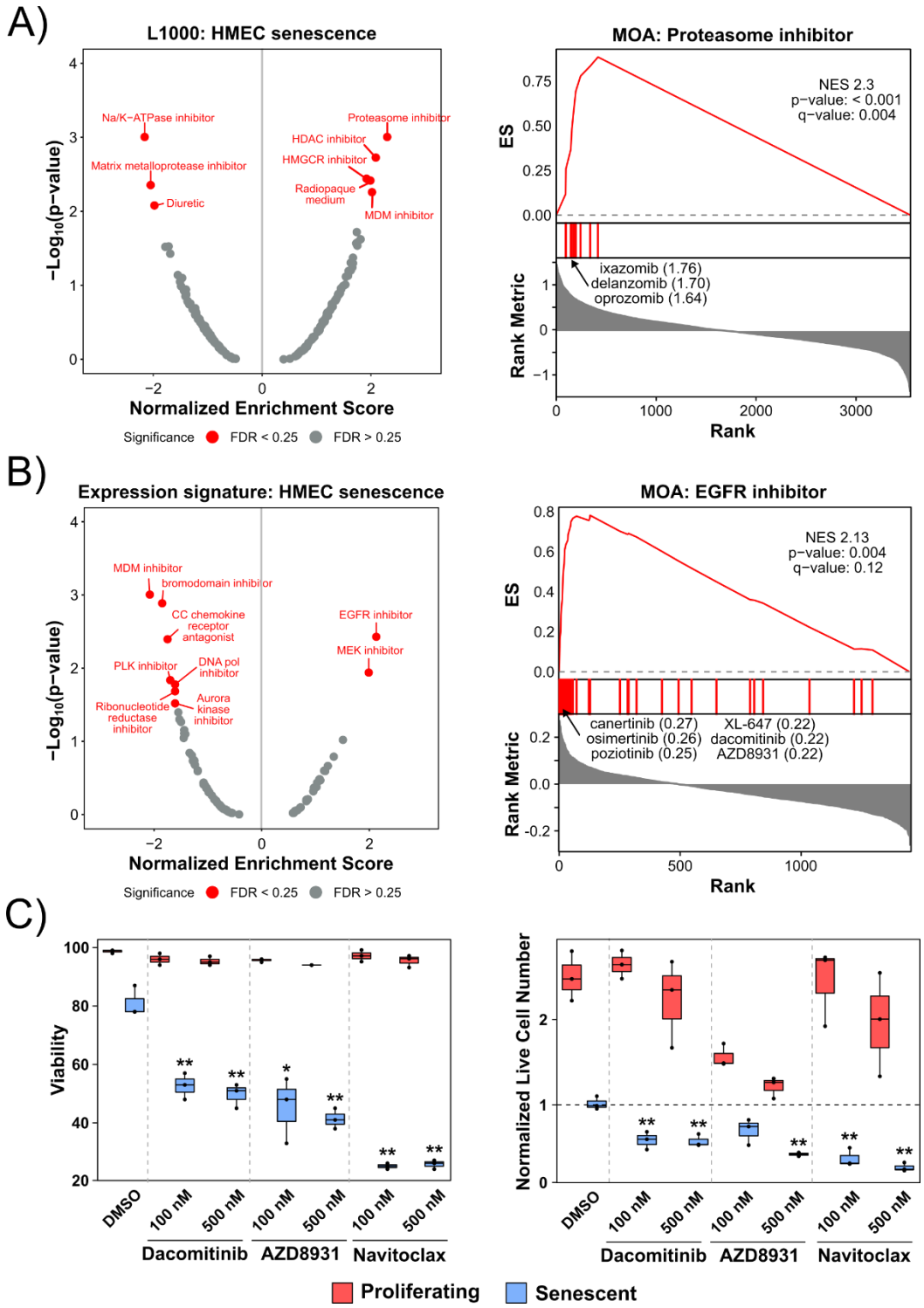

Figure 6. DMEA predicts senescence-inducing and senolytic drug MOAs for primary HMECs. A) Using a proteomic signature of replicative senescence in primary HMECs [34], we generated a rank-ordered drug list by querying the CMap L1000 database of perturbation signatures and then analyzed the output rank-ordered drug list by DMEA. (Left) Volcano plot of NES versus -$\log_{10}$(p-value) for drug MOAs from DMEA. Red text indicates MOAs with p-value <

0.05 and FDR < 0.25. (Right) Mountain plot showing the positive enrichment of the proteasome inhibitor MOA in the rank-ordered drug list of CMap L1000 connectivity scores. The proteasome inhibitors with the most positive connectivity scores are highlighted. B) The up- and down-regulated proteins from the same proteomic signature of HMEC replicative senescence [34] along with their $\log_2$ fold change values was used an input to our DMEA pipeline that calculates WGV scores using the external gene signature and then correlates WGV scores with drug toxicity from the PRISM database (Supp. Fig. 2). We then analyzed the output rank-ordered drug list by DMEA. (Left) Volcano plot of NES versus $-\log_{10}$(p-value) for drug MOAs from DMEA. Red text indicates MOAs with p-value < 0.05 and FDR < 0.25. (Right) Mountain plot showing the negative enrichment of the EGFR inhibitor MOA in the rank-ordered drug list of correlation coefficients. The EGFR inhibitors with the most negative correlation coefficients are highlighted. C) The EGFR inhibitors dacomitinib and AZD8931 and the senolytic compound navitoclax exhibited senolytic activity in HMECs. Proliferating HMECs (PD ~12) were treated with DMSO or 2 μM triapine for 3 days to induce proliferating or senescent phenotypes, respectively, as in our previous work [41]. Proliferating and senescent HMECs were then treated with DMSO (negative control), 100 nM / 500 nM dacomitinib, 100 nM / 500 nM AZD8931, or 100 / 500 nM navitoclax for 3 days, after which cell viability and live cell number were measured by trypan blue staining. The live cell number was normalized to the number of live cells present at the time of drug treatment. * and ** represent p < 0.05 and 0.01, respectively, compared to the senescent DMSO control calculated by Student's t-test.

DISCUSSION

Here, we introduce Drug Mechanism Enrichment Analysis (DMEA), a user-friendly bioinformatic method to identify enriched sets of drugs that share a common MOA in rank-ordered drug lists. Similar to how GSEA enhances biological interpretation of transcriptomic data [28], DMEA enables interpretation of rank-ordered drug lists by aggregating information from drugs with a common MOA, thereby avoiding problems inherent in the interpretation of single drug results. We have demonstrated the power and sensitivity of DMEA first with simulated data (Fig. 2) and then with real examples including gene expression connectivity scores (Fig. 3), cell viability connectivity scores (Fig. 4), and weighted gene voting molecular classification scores (Fig. 5). For all these test cases, DMEA successfully detected the expected MOA and highlighted other MOAs of interest. Finally, we used DMEA as a discovery tool to generate hypotheses about senescence-inducing and senolytic drug MOAs for primary HMECs and then experimentally validated the DMEA-generated hypothesis that EGFR inhibitors exhibit senolytic activity in HMECs. These

results demonstrate how DMEA can facilitate biological understanding of rank-ordered drug lists for drug discovery.

As such, DMEA can serve as a companion to other drug prediction methods that produce long, rank-ordered list of drugs that can be difficult to interpret. For example, when querying the CMap L1000 database of transcriptomic data, the output includes a folder labeled “GSEA” that contains a DMEA-like enrichment analysis of drug MOAs. However, we have not found any published description or online documentation of this CMap feature. In addition, we note that our DMEA application differs from the CMap drug MOA enrichment analysis in four significant ways. First, our DMEA application generates mountain plots which are essential to avoid false positive results in rank-based enrichment analyses [28]. Second, our DMEA application accepts any type of rank-ordered drug list, not just outputs from the L1000 analysis of perturbagen signatures. Third, the CMap MOA enrichment analysis tool produces an output list of >12,000 partially overlapping drug MOAs (e.g., 37 versions of MEK inhibitor MOA), whereas our DMEA application collapses drug responses to a more readily interpretable list of ~180 drug MOAs (i.e., only one MEK inhibitor MOA). Lastly, DMEA usually takes less than 1 minute to run, whereas the CMap Query tool often takes more than 1 hour. Thus, DMEA adds significant features and flexibility compared to the L1000 MOA enrichment analysis on the CMap web portal.

Notably, our validation results have demonstrated the flexibility of DMEA to analyze a variety of input rank-ordered drug lists and to identify enrichment of diverse MOAs (e.g., kinase inhibitors, proteasome inhibitors, metabolic pathway inhibitors). In these validation cases, DMEA not only identified the expected drug MOAs (e.g., EGFR inhibitor MOA given a signature of EGFR inhibitor resistance), but also MOAs which may exhibit toxicity against tumor cells resistant to the input signature of interest. One interesting example is that DMEA identified HMGCR inhibitors as toxic to cancer cells with intrinsic resistance to EGFR inhibitors (Fig. 5C). Indeed, this finding is

supported by published work demonstrating that HMGCR inhibitors can overcome resistance to EGFR inhibitors in NSCLC cells by inhibiting AKT [42,43]. In addition, DMEA also predicted that EGFR inhibitor-resistant cells would be sensitive to MDM inhibitors (Fig. 5A, Supp. Fig. 4C), a finding that is supported by published work showing that MDM2 mediates resistance to EGFR inhibitors in mouse models of NSCLC [44]. Furthermore, our analysis suggested that melanomas sensitive to BRAF inhibitors would also be sensitive to MEK inhibitors (Fig. 5D), an observation that is supported by clinical trials showing that combination treatment with BRAF and MEK inhibitors is more effective than inhibition of BRAF alone in BRAF-mutant melanoma patients [45]. Finally, for melanomas resistant to RAF inhibitors, DMEA identified CHK inhibitors as potentially beneficial. In fact, CHK1 inhibition has shown efficacy in melanoma xenografts and cell lines that are resistant to RAF inhibitors [46]. Collectively, these results support that DMEA can identify drug mechanisms beneficial for combination treatments and drug-resistant cancers.

Both senescence-inducing and senolytic compounds have emerged as an exciting area with great therapeutic promise in aging [47–51], cancer [52,53], and other diseases [54]. To demonstrate the power of DMEA for biological discovery, we used our recently published proteomic signature of replicative senescence in primary HMECs [34] as an input to DMEA (Fig. 6). Among the potential senescence-inducing drug MOAs identified by DMEA were proteasome, HDAC, HMGCR, and MDM inhibitors (Fig. 6A). Indeed, experimental evidence has shown that proteasome inhibitors induce senescence in primary fibroblasts [55,56] and that HDAC inhibitors can induce senescence in cancer cells [57–59]. In addition, we used the up- and down-regulated protein biomarkers of HMEC senescence to predict senolytic compounds. This analysis identified EGFR and MEK inhibitors as senolytic MOAs (Fig. 6B), which we subsequently experimentally validated with the EGFR inhibitors dacomitinib and AZD8931 in a drug-induced model of HMEC senescence (Fig. 6C). To our knowledge, this is the first demonstration that EGFR inhibitors can exhibit senolytic activity. Although we did not test whether MEK inhibitors would exhibit senolytic

activity in primary HMECs, it has been shown in Ras-expressing cells that MEK inhibitors selectively kill senescent cells [60]. Taken together, our results suggest that DMEA is a powerful tool for discovering novel drug MOAs with selectivity against molecularly characterized cell states.

Despite the success of our validation examples, we note that DMEA is limited by our knowledge of drug MOA annotations. For many targeted therapeutics, the putative MOA may be incorrect [61]. Nevertheless, DMEA mitigates the risk of false positives by evaluating groups of drugs which share a MOA rather than relying on results from single drugs. Thus, even if some drugs are misannotated, DMEA may still correctly identify enriched MOAs by aggregating information across multiple drugs, rather than considering individual drugs independently. However, improved annotation of drug MOAs and targets, potentially through newer approaches including metabolomics [62] and proteomics [63], will improve the power of DMEA.

In summary, Drug Mechanism Enrichment Analysis (DMEA) is a bioinformatic tool which identifies enriched drug MOAs in rank-ordered drug lists to facilitate biological understanding. Our approach leverages the dramatic growth in public databases of transcriptomic profiles (e.g., L1000, CCLE) and drug screens (e.g., PRISM) for cancer cell lines. When paired with a molecular classification method such as WGV, DMEA can even identify drug mechanisms which exhibit selectivity towards cell states (e.g., cancer, senescence) based on an input gene signature. We envision that the DMEA framework will be applicable to many biological contexts. DMEA is publicly available to use either as a web application or an R package at https://belindabgarana.github.io/DMEA.

FUNDING

This work was supported by the Viterbi School of Engineering. This material is based upon work supported by the National Science Foundation Graduate Research Fellowship Program under Grant No. DGE-1842487. Any opinions, findings, and conclusions or recommendations expressed in this material are those of the author(s) and do not necessarily reflect the views of the National Science Foundation.

REFERENCES

1. Li H, Ning S, Ghandi M, Kryukov GV, Gopal S, Deik A, et al. The landscape of cancer cell line metabolism. Nature Medicine. 2019;25: 850. doi:10.1038/s41591-019-0404-8

2. Nusinow DP, Szpyt J, Ghandi M, Rose CM, McDonald ER, Kalocsay M, et al. Quantitative Proteomics of the Cancer Cell Line Encyclopedia. Cell. 2020;180: 387-402.e16. doi:10.1016/j.cell.2019.12.023

3. Ghandi M, Huang FW, Jané-Valbuena J, Kryukov GV, Lo CC, McDonald ER, et al. Next-generation characterization of the Cancer Cell Line Encyclopedia. Nature. 2019;569: 503–508. doi:10.1038/s41586-019-1186-3

4. Frejno M, Meng C, Ruprecht B, Oellerich T, Scheich S, Kleigrewe K, et al. Proteome activity landscapes of tumor cell lines determine drug responses. Nature Communications. 2020;11: 3639. doi:10.1038/s41467-020-17336-9

5. Corsello SM, Nagari RT, Spangler RD, Rossen J, Kocak M, Bryan JG, et al. Discovering the anticancer potential of non-oncology drugs by systematic viability profiling. Nat Cancer. 2020;1: 235–248. doi:10.1038/s43018-019-0018-6

6. Behan FM, Iorio F, Picco G, Gonçalves E, Beaver CM, Migliardi G, et al. Prioritization of cancer therapeutic targets using CRISPR–Cas9 screens. Nature. 2019;568: 511–516. doi:10.1038/s41586-019-1103-9

7. Meyers RM, Bryan JG, McFarland JM, Weir BA, Sizemore AE, Xu H, et al. Computational correction of copy number effect improves specificity of CRISPR–Cas9 essentiality screens in cancer cells. Nat Genet. 2017;49: 1779–1784. doi:10.1038/ng.3984

8. Subramanian A, Narayan R, Corsello SM, Peck DD, Natoli TE, Lu X, et al. A Next Generation Connectivity Map: L1000 Platform and the First 1,000,000 Profiles. Cell. 2017;171: 1437-1452.e17. doi:10.1016/j.cell.2017.10.049

9. Parca L, Pepe G, Pietrosanto M, Galvan G, Galli L, Palmeri A, et al. Modeling cancer drug response through drug-specific informative genes. Sci Rep. 2019;9: 15222. doi:10.1038/s41598-019-50720-0

10. Wei D, Liu C, Zheng X, Li Y. Comprehensive anticancer drug response prediction based on a simple cell line-drug complex network model. BMC Bioinformatics. 2019;20: 44. doi:10.1186/s12859-019-2608-9

11. Suphavilai C, Bertrand D, Nagarajan N. Predicting Cancer Drug Response using a Recommender System. Bioinformatics. 2018;34: 3907–3914. doi:10.1093/bioinformatics/bty452

12. Yuan H, Paskov I, Paskov H, González AJ, Leslie CS. Multitask learning improves prediction of cancer drug sensitivity. Sci Rep. 2016;6: 31619. doi:10.1038/srep31619

13. Choi J, Park S, Ahn J. RefDNN: a reference drug based neural network for more accurate prediction of anticancer drug resistance. Sci Rep. 2020;10: 1861. doi:10.1038/s41598-020-58821-x

14. Gonçalves E, Segura-Cabrera A, Pacini C, Picco G, Behan FM, Jaaks P, et al. Drug mechanism-of-action discovery through the integration of pharmacological and CRISPR screens. Molecular Systems Biology. 2020;16: e9405. doi:10.15252/msb.20199405

15. Nguyen L, Dang CC, Ballester PJ. Systematic assessment of multi-gene predictors of pan-cancer cell line sensitivity to drugs exploiting gene expression data. F1000Res. 2017;5: ISCB Comm J-2927. doi:10.12688/f1000research.10529.2

16. Gao S, Han L, Luo D, Liu G, Xiao Z, Shan G, et al. Modeling drug mechanism of action with large scale gene-expression profiles using GPAR, an artificial intelligence platform. BMC Bioinformatics. 2021;22: 17. doi:10.1186/s12859-020-03915-6

17. Napolitano F, Carrella D, Mandriani B, Pisonero-Vaquero S, Sirci F, Medina DL, et al. gene2drug: a computational tool for pathway-based rational drug repositioning. Bioinformatics. 2018;34: 1498–1505. doi:10.1093/bioinformatics/btx800

18. Fang M, Richardson B, Cameron CM, Dazard J-E, Cameron MJ. Drug perturbation gene set enrichment analysis (dpGSEA): a new transcriptomic drug screening approach. BMC Bioinformatics. 2021;22: 22. doi:10.1186/s12859-020-03929-0

19. Prinz J, Vogt I, Adornetto G, Campillos M. A Novel Drug-Mouse Phenotypic Similarity Method Detects Molecular Determinants of Drug Effects. PLOS Computational Biology. 2016;12: e1005111. doi:10.1371/journal.pcbi.1005111

20. Malyutina A, Majumder MM, Wang W, Pessia A, Heckman CA, Tang J. Drug combination sensitivity scoring facilitates the discovery of synergistic and efficacious drug combinations in cancer. PLOS Computational Biology. 2019;15: e1006752. doi:10.1371/journal.pcbi.1006752

21. Gayvert KM, Aly O, Platt J, Bosenberg MW, Stern DF, Elemento O. A Computational Approach for Identifying Synergistic Drug Combinations. PLOS Computational Biology. 2017;13: e1005308. doi:10.1371/journal.pcbi.1005308

22. Rivas-Barragan D, Mubeen S, Bernat FG, Hofmann-Apitius M, Domingo-Fernández D. Drug2ways: Reasoning over causal paths in biological networks for drug discovery. PLOS Computational Biology. 2020;16: e1008464. doi:10.1371/journal.pcbi.1008464

23. Domingo-Fernández D, Gadiya Y, Patel A, Mubeen S, Rivas-Barragan D, Diana CW, et al. Causal reasoning over knowledge graphs leveraging drug-perturbed and disease-specific transcriptomic signatures for drug discovery. PLOS Computational Biology. 2022;18: e1009909. doi:10.1371/journal.pcbi.1009909

24. Brum AM, van de Peppel J, van der Leije CS, Schreuders-Koedam M, Eijken M, van der Eerden BCJ, et al. Connectivity Map-based discovery of parbendazole reveals targetable human osteogenic pathway. Proceedings of the National Academy of Sciences. 2015;112: 12711–12716. doi:10.1073/pnas.1501597112

25. Zhang M, Luo H, Xi Z, Rogaeva E. Drug Repositioning for Diabetes Based on “Omics” Data Mining. PLOS ONE. 2015;10: e0126082. doi:10.1371/journal.pone.0126082

26. Tsoi J, Robert L, Paraiso K, Galvan C, Sheu KM, Lay J, et al. Multi-stage Differentiation Defines Melanoma Subtypes with Differential Vulnerability to Drug-Induced Iron-Dependent Oxidative Stress. Cancer Cell. 2018;33: 890-904.e5. doi:10.1016/j.ccell.2018.03.017

27. Viswanathan VS, Ryan MJ, Dhruv HD, Gill S, Eichhoff OM, Seashore-Ludlow B, et al. Dependency of a therapy-resistant state of cancer cells on a lipid peroxidase pathway. Nature. 2017;547: 453–457. doi:10.1038/nature23007

28. Subramanian A, Tamayo P, Mootha VK, Mukherjee S, Ebert BL, Gillette MA, et al. Gene set enrichment analysis: A knowledge-based approach for interpreting genome-wide expression profiles. Proceedings of the National Academy of Sciences. 2005;102: 15545–15550. doi:10.1073/pnas.0506580102

29. Maejima T, Inoue T, Kanki Y, Kohro T, Li G, Ohta Y, et al. Direct evidence for pitavastatin induced chromatin structure change in the KLF4 gene in endothelial cells. PLoS One. 2014;9: e96005. doi:10.1371/journal.pone.0096005

30. Greger JG, Eastman SD, Zhang V, Bleam MR, Hughes AM, Smitheman KN, et al. Combinations of BRAF, MEK, and PI3K/mTOR inhibitors overcome acquired resistance to the BRAF inhibitor GSK2118436 dabrafenib, mediated by NRAS or MEK mutations. Mol Cancer Ther. 2012;11: 909–920. doi:10.1158/1535-7163.MCT-11-0989

31. Wang Q, Mora-Jensen H, Weniger MA, Perez-Galan P, Wolford C, Hai T, et al. ERAD inhibitors integrate ER stress with an epigenetic mechanism to activate BH3-only protein NOXA in cancer cells. Proc Natl Acad Sci U S A. 2009;106: 2200–2205. doi:10.1073/pnas.0807611106

32. Narla A, Dutt S, McAuley JR, Al-Shahrour F, Hurst S, McConkey M, et al. Dexamethasone and lenalidomide have distinct functional effects on erythropoiesis. Blood. 2011;118: 2296–2304. doi:10.1182/blood-2010-11-318543

33. Brachmann SM, Kleylein-Sohn J, Gaulis S, Kauffmann A, Blommers MJJ, Kazic-Legueux M, et al. Characterization of the mechanism of action of the pan class I PI3K inhibitor NVP-BKM120 across a broad range of concentrations. Mol Cancer Ther. 2012;11: 1747–1757. doi:10.1158/1535-7163.MCT-11-1021

34. Delfarah A, Hartel NG, Zheng D, Yang J, Graham NA. Identification of a Proteomic Signature of Senescence in Primary Human Mammary Epithelial Cells. J Proteome Res. 2021;20: 5169–5179. doi:10.1021/acs.jproteome.1c00659

35. Golub TR, Slonim DK, Tamayo P, Huard C, Gaasenbeek M, Mesirov JP, et al. Molecular Classification of Cancer: Class Discovery and Class Prediction by Gene Expression Monitoring. Science. 1999;286: 531–537. doi:10.1126/science.286.5439.531

36. Ritchie ME, Phipson B, Wu D, Hu Y, Law CW, Shi W, et al. limma powers differential expression analyses for RNA-sequencing and microarray studies. Nucleic Acids Research. 2015;43: e47–e47. doi:10.1093/nar/gkv007

37. Hoeflich KP, O'Brien C, Boyd Z, Cavet G, Guerrero S, Jung K, et al. In vivo antitumor activity of MEK and phosphatidylinositol 3-kinase inhibitors in basal-like breast cancer models. Clin Cancer Res. 2009;15: 4649–4664. doi:10.1158/1078-0432.CCR-09-0317

38. Balko JM, Potti A, Saunders C, Stromberg A, Haura EB, Black EP. Gene expression patterns that predict sensitivity to epidermal growth factor receptor tyrosine kinase inhibitors in lung cancer cell lines and human lung tumors. BMC Genomics. 2006;7: 289. doi:10.1186/1471-2164-7-289

39. Coldren CD, Helfrich BA, Witta SE, Sugita M, Lapadat R, Zeng C, et al. Baseline Gene Expression Predicts Sensitivity to Gefitinib in Non–Small Cell Lung Cancer Cell Lines. Mol Cancer Res. 2006;4: 521–528. doi:10.1158/1541-7786.MCR-06-0095

40. Kemper K, Krijgsman O, Kong X, Cornelissen-Steijger P, Shahrabi A, Weeber F, et al. BRAF(V600E) Kinase Domain Duplication Identified in Therapy-Refractory Melanoma Patient-Derived Xenografts. Cell Rep. 2016;16: 263–277. doi:10.1016/j.celrep.2016.05.064

41. Delfarah A, Parrish S, Junge JA, Yang J, Seo F, Li S, et al. Inhibition of nucleotide synthesis promotes replicative senescence of human mammary epithelial cells. J Biol Chem. 2019; jbc.RA118.005806. doi:10.1074/jbc.RA118.005806

42. Hwang K-E, Kwon S-J, Kim Y-S, Park D-S, Kim B-R, Yoon K-H, et al. Effect of simvastatin on the resistance to EGFR tyrosine kinase inhibitors in a non-small cell lung cancer with the T790M mutation of EGFR. Experimental Cell Research. 2014;323: 288–296. doi:10.1016/j.yexcr.2014.02.026

43. Chen J, Bi H, Hou J, Zhang X, Zhang C, Yue L, et al. Atorvastatin overcomes gefitinib resistance in KRAS mutant human non-small cell lung carcinoma cells. Cell Death Dis. 2013;4: e814–e814. doi:10.1038/cddis.2013.312

44. Shen H, Wang G-C, Li X, Ge X, Wang M, Shi Z-M, et al. S6K1 blockade overcomes acquired resistance to EGFR-TKIs in non-small cell lung cancer. Oncogene. 2020;39: 7181–7195. doi:10.1038/s41388-020-01497-4

45. Long GV, Stroyakovskiy D, Gogas H, Levchenko E, de Braud F, Larkin J, et al. Combined BRAF and MEK inhibition versus BRAF inhibition alone in melanoma. N Engl J Med. 2014;371: 1877–1888. doi:10.1056/NEJMoa1406037

46. Hwang B-J, Adhikary G, Eckert RL, Lu A-L. Chk1 inhibition as a novel therapeutic strategy in melanoma. Oncotarget. 2018;9: 30450–30464. doi:10.18632/oncotarget.25765

47. Xu M, Pirtskhalava T, Farr JN, Weigand BM, Palmer AK, Weivoda MM, et al. Senolytics improve physical function and increase lifespan in old age. Nature Medicine. 2018;24: 1246–1256. doi:10.1038/s41591-018-0092-9

48. Baar MP, Brandt RMC, Putavet DA, Klein JDD, Derks KWJ, Bourgeois BRM, et al. Targeted Apoptosis of Senescent Cells Restores Tissue Homeostasis in Response to Chemotoxicity and Aging. Cell. 2017;169: 132-147.e16. doi:10.1016/j.cell.2017.02.031

49. Baker DJ, Wijshake T, Tchkonia T, LeBrasseur NK, Childs BG, van de Sluis B, et al. Clearance of p16Ink4a-positive senescent cells delays ageing-associated disorders. Nature. 2011;479: 232–236. doi:10.1038/nature10600

50. Baker DJ, Childs BG, Durik M, Wijers ME, Sieben CJ, Zhong J, et al. Naturally occurring p16 Ink4a -positive cells shorten healthy lifespan. Nature. 2016;530: 184–189. doi:10.1038/nature16932

51. Cai Y, Zhou H, Zhu Y, Sun Q, Ji Y, Xue A, et al. Elimination of senescent cells by β-galactosidase-targeted prodrug attenuates inflammation and restores physical function in aged mice. Cell Research. 2020;30: 574–589. doi:10.1038/s41422-020-0314-9

52. Dörr JR, Yu Y, Milanovic M, Beuster G, Zasada C, Däbritz JHM, et al. Synthetic lethal metabolic targeting of cellular senescence in cancer therapy. Nature. 2013;501: 421–425. doi:10.1038/nature12437

53. Guerrero A, Herranz N, Sun B, Wagner V, Gallage S, Guiho R, et al. Cardiac glycosides are broad-spectrum senolytics. Nat Metab. 2019;1: 1074–1088. doi:10.1038/s42255-019-0122-z

54. Hickson LJ, Langhi Prata LGP, Bobart SA, Evans TK, Giorgadze N, Hashmi SK, et al. Senolytics decrease senescent cells in humans: Preliminary report from a clinical trial of Dasatinib plus Quercetin in individuals with diabetic kidney disease. EBioMedicine. 2019;47: 446–456. doi:10.1016/j.ebiom.2019.08.069

55. Chondrogianni N, Gonos ES. Proteasome inhibition induces a senescence-like phenotype in primary human fibroblasts cultures. Biogerontology. 2004;5: 55–61. doi:10.1023/B:BGEN.0000017687.55667.42

56. Torres C, Lewis L, Cristofalo VJ. Proteasome inhibitors shorten replicative life span and induce a senescent-like phenotype of human fibroblasts. Journal of Cellular Physiology. 2006;207: 845–853. doi:10.1002/jcp.20630

57. Lorenz V, Hessenkemper W, Rödiger J, Kyrylenko S, Kraft F, Baniahmad A. Sodium butyrate induces cellular senescence in neuroblastoma and prostate cancer cells. Horm Mol Biol Clin Investig. 2011;7: 265–272. doi:10.1515/HMBCI.2011.020

58. Venkatesh R, Ramaiah MJ, Gaikwad HK, Janardhan S, Bantu R, Nagarapu L, et al. Luotonin-A based quinazolinones cause apoptosis and senescence via HDAC inhibition and activation of tumor suppressor proteins in HeLa cells. Eur J Med Chem. 2015;94: 87–101. doi:10.1016/j.ejmech.2015.02.057

59. Vargas JE, Filippi-Chiela EC, Suhre T, Kipper FC, Bonatto D, Lenz G. Inhibition of HDAC increases the senescence induced by natural polyphenols in glioma cells. Biochem Cell Biol. 2014;92: 297–304. doi:10.1139/bcb-2014-0022

60. Kochetkova EY, Blinova GI, Bystrova OA, Martynova MG, Pospelov VA, Pospelova TV. Targeted elimination of senescent Ras-transformed cells by suppression of MEK/ERK pathway. Aging (Albany NY). 2017;9: 2352–2375. doi:10.18632/aging.101325

61. Lin A, Giuliano CJ, Palladino A, John KM, Abramowicz C, Yuan ML, et al. Off-target toxicity is a common mechanism of action of cancer drugs undergoing clinical trials. Science Translational Medicine. 2019;11. doi:10.1126/scitranslmed.aaw8412

62. Holbrook-Smith D, Durot S, Sauer U. High-throughput metabolomics predicts drug-target relationships for eukaryotic proteins. Mol Syst Biol. 2022;18: e10767. doi:10.15252/msb.202110767

63. Savitski MM, Reinhard FBM, Franken H, Werner T, Savitski MF, Eberhard D, et al. Tracking cancer drugs in living cells by thermal profiling of the proteome. Science. 2014 [cited 31 Jan 2022]. doi:10.1126/science.1255784